9-19-2018

Evolution of grain size distributions and bed mobility during hydrographs in gravel-bed braided rivers

Sarah Peirce

Peter Ashmore
pashmore@uwo.ca

Pauline Leduc

Earth Surface Processes and Landforms BSG British Society for Geomorphology

Evolution of Grain Size Distributions and Bed Mobility during Hydrographs in Gravel-Bed Braided Rivers

Journal:	*Earth Surface Processes and Landforms*
Manuscript ID	ESP-17-0361.R2
Wiley - Manuscript type:	Research Article
Date Submitted by the Author:	23-Aug-2018

Complete List of Authors:	Peirce, Sarah; The University of Western Ontario, Geography Ashmore, Peter; University of Western Ontario, Geography Leduc, Pauline; Western University, Department of Geography

Keywords:	Braided river, Physical model, bed mobility, grain size, gravel-bed

Evolution of Grain Size Distributions and Bed Mobility during Hydrographs in Gravel-Bed Braided Rivers

S. Peirce[1], P. Ashmore[1], and P. Leduc[1]

[1]University of Western Ontario, London, Ontario, Canada

Corresponding author: Sarah Peirce (speirce@uwo.ca)

Key Points:

The transition from partial to selective mobility in physical models of gravel-bed braiding rivers corresponds to the lower threshold of substantial morphological change and bedload transport and occurs at approximately 50% of peak channel-forming discharge, or dimensionless stream power of 70. The expansion of the morphological active depth and morphological active width with increasing discharge is directly related to the mobilization of the coarsest grain size fractions, indicating that bedload grain size distributions, while tied to hydraulic forcing, are also related to braiding morphodynamics.

Abstract

Evolution of bed material mobility and bedload grain size distributions under a range of discharges is rarely observed in braiding in gravel-bed rivers. Yet, the changing of bedload grain size distributions with discharge is expected to be different from laterally-stable, threshold, channels on which most gravel bedload theory and observation are based. Here, simultaneous observations of flow, bedload transport rate, and morphological change were made in a physical model of a gravel-bed braided river to document the evolution of grain size distributions and bed mobility over three experimental event hydrographs. Bedload transport rate and grain size distributions were measured from bedload samples collected in sediment baskets. Morphological change was mapped with high-resolution (~1 mm precision) digital elevation models generated from close-range digital photogrammetry. Bedload transport rates were extremely low below a discharge equivalent to ~50 % of the channel-forming discharge (dimensionless stream power ~70). Fractional transport rates and plots of grain size distributions indicate that the bed experienced partial mobility at low discharge when the coarsest grains on the bed were immobile, weak selective mobility at higher discharge, and occasionally near-equal mobility at peak channel-forming discharge. The transition to selective mobility and increased bedload transport rates coincided with the lower threshold for morphological change measured by the morphological active depth and active width. Below this threshold discharge, active depths were of the order of D_{90} and active widths narrow (< 3% of wetted width). Above this discharge, both increased so that at channel-forming discharge, the active depth had a local maximum of $9D_{90}$ while active width was up to 20% of wetted width. The modelled rivers approached equal mobility when rates of

morphological change were greatest. Therefore, changes in the morphological active layer with discharge is directly connected to the conditions bed mobility, and strongly correlated with bedload transport rate.

Introduction

The relationships between bedload grain size distributions (GSD), bed mobility, and channel morphology in gravel-bed rivers have important implications for the basic understanding of river dynamics as well as many practical applications. For example, this data can be used to estimate bedload sediment yield and channel stability, which in turn are used to inform channel, reservoir, and infrastructure design (Powell et al., 2001b; Ryan et al., 2002). In addition, GSD and bed mobility data are necessary for the effective numerical modelling of sediment entrainment and channel morphodynamics (Powell et al., 2001b; Wilcock and McArdell, 1997a; Williams et al., 2016a, 2016b) and can help define the disturbance regimes and substrate quality of gravel-bed rivers for benthic organisms and fish (Haschenburger and Wilcock, 2003; Wilcock and McArdell, 1997a).

Individual grain size fractions in gravel bed rivers are defined as fully mobilized when the entire population of that grain size available for transport in the bed material is entrained during a flow event, otherwise the fraction is only partially mobilized (Haschenburger and Wilcock, 2003; Wilcock and McArdell, 1997b). With regards to the channel bed as a whole, three main mobility states have been defined for gravel-bed rivers: partial mobility, selective mobility, and equal mobility (Parker, 2008; Venditti et al., 2017). Partial mobility occurs when the GSD of the bedload is finer than that of the bed because some coarse fractions on the bed surface remain immobile, even during high flows. Selective mobility occurs when all of the grain sizes on the surface are found in the bedload, but not in proportion to their availability on the bed, reflecting a mix of fully mobilized and partially mobilized grain size fractions. Finally, equal mobility occurs when the GSD of the bedload and bed material are identical (i.e., all grain size fractions are fully mobilized in proportion to their availability).

While many studies have investigated changes in grain size and bed mobility for single-thread gravel-bed rivers or in narrow, straight-walled flumes, there is comparatively little research on these processes in braiding rivers (Ashworth et al., 1992; Ashworth and Ferguson, 1986, 1989; Kociuba and Janicki, 2015; Mao and Surian, 2010). Defined by their multiple anabranch channels and ephemeral bars, braided rivers have a complex morphology producing spatially and temporally variable bedload transport rates commonly observed in the field (Ashworth and Ferguson, 1986; Mao and Surian, 2010; Powell and Ashworth, 1995; Williams et al., 2015b) and in physical models (Ashmore, 1988; Ashmore and Church, 1998; Hoey, 1992; Hoey and Sutherland, 1991). While there has been some success characterizing bedload transport functions at the reach scale using temporal averages (Ashmore, 1988; Bertoldi et al., 2009; Williams et al., 2016a), the complex morphology and hydraulics as well as rapid morphological change makes bedload transport rates and bed material mobility in braided rivers inherently difficult to measure directly, or to predict using classic hydraulically-driven bedload functions (Bertoldi et al., 2009; Davies, 1987; Kociuba and Janicki, 2015; Mao and Surian, 2010; Powell and Ashworth, 1995; Recking et al., 2016).

Though not thoroughly investigated in the past, bedload transport and mobility of bed material particle size fractions over a range of discharges in braided rivers may behave differently than laterally stable single-threaded channels for several reasons. First, braided rivers are often characterized by high sediment supply relative to bedload transport capacity (Ferguson, 1987; Mueller and Pitlick, 2013, 2014). High rates of lateral migration (i.e., bank and bar erosion) and an extensive morphological active layer (Ashmore et al., 2018) provide locally high rates of sediment input to bedload transport (Wheaton et al., 2013; Williams et al., 2015b) at the channel scale in combination with high rates of sediment supply provided at the watershed scale (Guerit et al., 2014; Mueller and Pitlick, 2014; Piegay et al., 2006). As a consequence, braided rivers often lack strong surface armour (Bunte and Abt, 2001; Gardner and Ashmore, 2011a; Gardner et al., 2017; Guerit et al., 2014; Leduc et al., 2015; Mueller and Pitlick, 2013, 2014) and differences in surface and subsurface GSDs may be small (Carson and Griffiths, 1987; Laronne et al., 1994; Laronne and Reid, 1993; Lisle, 1995; Lisle et al., 2000; Mueller and Pitlick, 2013) unlike typical stable, single-thread gravel-bed rivers that often have a distinct coarse surface layer relative to the subsurface sediment. At the same time, braided rivers exhibit a wide range of bed material particle sizes available at the bed surface due to processes like strong lateral sorting effects around bars (Ashworth and Ferguson, 1986; Bluck, 1979; Leduc et al., 2015; Smith, 1974). Furthermore, recent research has shown no significant vertical sorting within braided river deposits and that the morphological active depth (i.e. vertical depth of morphological change and bed material turnover) extends to several multiples of the surface D90, making it possible to mobilize large portions of the subsurface material during active braiding (Ashmore et al., 2018; Gardner and Ashmore, 2011b; Gardner et al., 2017; Leduc et al., 2015). Second, and following from this, braided rivers actively rework large areas of the bed over short time periods (e.g., single flow events) (Ashmore, 2013; Ashmore et al., 2018; Leduc et al., 2015; Wheaton et al., 2013; Williams et al., 2015a, 2016a, 2016b). This occurs in part because the area of the bed that is wetted and experiencing active bedload transport (i.e. the morphological active width) increases rapidly with discharge in braided rivers (Ashmore et al., 2011; Lugo et al., 2015; Peirce et al., 2018). The lateral adjustment of the morphological active width with discharge is a significant component of bed material transport in braiding rivers (Bertoldi et al., 2009; Peirce et al., 2018; Williams et al., 2015b) that aids in the accessibility of a wide range of bed material particle sizes, both laterally and from the subsurface. These processes differ from more-stable, single-threaded channels, which can have immobile areas of the bed that persist for years (Haschenburger and Wilcock, 2003) and in which bedload mechanics are dominated by particle exchange at the bed with limited active layer depth (Church and Haschenburger, 2017). Overall, these differences between braiding and stable single channels may have important implications for predicting fractional and total transport rates and bed mobility. While most gravel-bed rivers are restricted to low transport rates and partial mobility due to surface armour (Church and Hassan, 2002; Venditti et al., 2017), braided rivers may be able to mobilize large areas and volumes of bed material as well as wide range of grain sizes (Ashworth and Ferguson, 1986, 1989; Mueller and Pitlick, 2014; Powell et al., 2001a) and consequently may show a different response to discharge than stable, near-threshold channels (*see* Church, 2006). However, there are very few data available for bedload particle mobility in gravel braided rivers. Ashworth and Ferguson (1986; 1989) observed that at the highest flows in a pro-glacial braided outwash, the particle size distribution of the bedload began to approach that of the braidplain deposits as a whole, although never reaching true equal mobility, and that mobility was greater in this actively braiding river than in two other more-stable rivers (Ashworth and Ferguson, 1989). Lisle (1995) found that, for a range of gravel bed river types, those with high average active layer depths (e.g., 4-12 x D_{84}), in which large areas of the streambed are mobilized during bedload transport events, had the greatest tendency to approach conditions of equal mobility and a braiding morphology.

Overall, it is expected that gravel-bed braided rivers may evolve towards full mobilization of coarse grains and equal mobility of the bed differently and at lower discharges (relative to 'bankfull') than more-stable, single-thread gravel-bed rivers. This evolution is likely to be associated with periods of rapid morphological change, and an extensive morphological active layer, both laterally and vertically (Ashmore et al., 2018). Yet, due to the demand for simultaneous measurements of bedload transport flux and morphological change, which would be practically impossible to collect in the field, these relationships between bedload and morphological change have not been systematically investigated in gravel-bed braided rivers. Here, we used a small-scale physical model of a gravel-bed braided river to obtain measurements of bedload transport rates, bedload grain size distributions, and morphological change over three experimental hydrographs reproducing diurnal meltwater discharge variation in a pro-glacial braided river. The use of a physical model allowed for bedload to be collected in traps at the outlet of the model while concurrent measurements of morphological change were determined via differencing of high-resolution and high-frequency digital elevation models (DEMs) (Brasington et al., 2000; Kasprak et al., 2015; Morgan et al., 2016). Therefore, we can quantitatively link changes in bedload transport and GSDs with changes in discharge, as well as the morphological active depth and the morphological active width in a braided

153 river. This makes it possible to investigate bed material mobility as a component of the intrinsically morphological process of bedload transport in braided rivers (Ashmore et al., 2011, 2018; Ashmore and Church, 1998; Bertoldi et al., 2009) and to characterize an aspect of gravel-bed braiding river dynamics and bedload transport in a manner not previously accomplished.

Methods

Physical Model

Data were gathered from hydrograph experiments using a Froude-scaled physical model of a gravel-bed braided river in a large river modelling flume (18.3 m x 3 m) with adjustable slope and discharge and recirculating water. Froude-scale modelling preserves dynamic similarity so that fundamental force ratios, particularly non-dimensional bed shear stress, are preserved and therefore both bedload transport and morphodynamic processes are modelled (Ashmore, 1982; Young and Warburton, 1996). Reduced scale models of this kind have been used extensively in research on gravel-bed braiding rivers (Ashmore, 1988, 1982; Warburton and Davies, 1994) and in fundamental research on gravel bed armoring and bed material mobility (Dietrich et al., 1989; Parker and Klingeman, 1982; Parker and Toro-Escobar, 2002). The GSD for the model was taken as the average subsurface GSD measured by sieving volumetric bulk samples from the model (Church and Hassan, 2002; Guerit et al., 2014). The grain sizes in the model ranged from 0.1-8 mm with D_{10} = 0.32 mm D_{50} = 1.18 mm and D_{90} = 3.52 mm. This is approximately a 1:35 scale of the bulk distribution from the Sunwapta River, a proglacial gravel-bed braided river in Alberta, Canada (D_{50} = 41 mm) (Figure 1) (Ashmore et al., 2011; Chew and Ashmore, 2001). The model distribution was truncated at approximately 0.25 mm (equivalent to 8 mm at full scale) to avoid cohesive grain effects and preserve similarity in flow resistance and bed morphology between the prototype and the model (Young and Warburton, 1996). Bedload was collected in five metal sediment baskets, with a mesh size of 0.1 mm, which spanned the entire width of the model at the outlet.

Experimental Procedure

A generic braided morphology was self-generated from an initially straight channel at a constant channel-forming discharge of 2.1 Ls^{-1} (± 5 %) and a slope of 1.5 %, which approximates the slope of a reach of the Sunwapta River (Chew and Ashmore, 2001). Following 24 hours of initial evolution to a braided morphology, three event hydrograph experiments (referred to as A, B, and C) were completed (Figure 2). Discharges were chosen to cover the range of discharges in a typical daily meltwater hydrograph of the Sunwapta River so that the channel-forming discharge and peak flow of 2.1 Ls^{-1} approximates the average diurnal peak discharge (15 m^3s^{-1}) in the prototype based on the 1:35 scaling ratio and Froude scaling of discharge (Ashmore and Sauks, 2006; Egozi and Ashmore, 2008). Each discharge step was run for at least 1 hour, split into 15 or 30 minute intervals for a total of 117 experimental runs and 27 discharge steps (Figure 2). The time intervals were chosen to obtain a high temporal frequency of surveying while still allowing for detectable morphological change to occur (Ashmore and Church, 1998), so all runs were 15 minutes except for several at the lowest discharge (0.7 Ls^{-1}), which were 30 minutes. The time base of a typical pro-glacial diurnal hydrograph is not reproduced in the tests because of the experimental need to keep each step in the hydrograph similar, at least 15 minutes long, and to focus on particle mobility and braiding morpho-dynamics across the discharge range.

At the end of each experimental run, the flow was turned off and once water was no longer flowing over the downstream end, the bedload trapped in the downstream sediment baskets was weighed using a load cell (precision ± 0.5 %) and then collected in sampling bags. The waning flow phase may have introduced very minor amounts of additional sediment into the baskets but these additions are expected to be negligible and consistent across all measurements due to the relatively short waning period. Once the model surface was drained of all standing water, high-resolution images of the dry bed surface were taken for DEM generation via digital photogrammetry (discussed below). To preserve the overall sediment balance of the model, a compensating volume of dry sediment with the same GSD as the model subsurface was fed into the tail tank at the end of each run to be fed into upstream end by a recirculating sediment pump during the subsequent run. Therefore, the GSD of the sediment fed into the model during each run was independent of the bedload collected during the previous run. Once the experiments were completed, the collected bedload samples were dried and sieved at intervals of 0.5 phi from -2.5 to 2 phi (5.6 - 0.25 mm).

Digital Photogrammetry: DEM Generation and Differencing

Digital photos of the dry model surface were taken using 2 T5i Canon cameras with 20 mm lenses mounted on a movable trolley ~2.9-3 m above the model surface (depending on exact location above the tilted flume). The camera orientation was slightly oblique so that the images from each camera were fully-convergent across the flume. Images were captured at approximately 0.4 m spacing along the flume (approximately 80% overlap of successive images). Nominal pixel resolution on the sand surface was 0.7mm. Coded targets (surveyed with sub-millimeter precision using a 2 second total station and 3D intersection calculation) in the model allowed for photos to be batch-processed using the Structure-from-Motion software program, Agisoft PhotoScan, which was used to generate orthophotos and DEMs of each surface with a 1.5 mm cell resolution and a vertical error estimate of (± 1.15 mm). This error estimate was based on an analysis of range of elevation differences in stable, flat areas of the model surface across all the DEMs. Example DEMs from the beginning of each hydrograph can be seen in Figure 3.

The open-source software program Scilab was used for DEM differencing, so that areas and volumes of topographic change could be quantified from the DEMs of Difference (DoD). A simple uniform threshold for change detection of 3.6 mm, which corresponds with 3 standard deviations of the vertical error estimate of the final DEM surfaces (± 1.15 mm), was applied to each DEM of Difference (DoD) followed by a dilation filter, which created a mask of 'change' (1) and 'no-change' (0). After the mask was applied to the raw DoD, a final uniform threshold of 1mm, which corresponds with the approximate D_{50} of the model, was applied. Therefore, the dilation method considers the neighbouring cells of areas with a high probability of 'real change', thereby improving connectivity between areas of morphological change while still reducing noise in the data. Each DoD was cropped to remove targets and inlet effects, so that the final study area was restricted to the downstream 14 m of the model. Reach-averaged estimates of the morphological active depth and morphological active width were derived for each run by dividing the total volume of change by the total active area, and dividing the total active area by the reach length (i.e., 14 m), respectively. In addition, reach-averaged wetted widths were measured from manually digitized orthophotos of the water surface using ArcMap 10.4. Finally, image texture analysis was used to map bed surface texture as a surrogate for bed material particle size at the beginning of each hydrograph, The method used was based on a technique developed by Carbonneau et al., (2005) and described by Leduc et al., (2015) for the same flume and bed sediment. The resulting data for "equivalent texture" (Leduc et al., 2015) was a calibrated equivalent to the median particle size in a 7 x7 pixel moving window that provides a relative measure of differences in bed material size spatially on the bed of the physical models.

Results

Bedload Transport Rate

Bedload transport rate (Q_b) ranged from 0.02- 11.70 gs^{-1} (Figure 4). The mean bedload transport rate and variability in transport rates increased with discharge so that the lowest discharge of 0.7 $l\ s^{-1}$ had the lowest mean transport rate of 0.12 gs^{-1} (standard deviation, $\sigma = 0.10$) and the highest discharge (2.1 Ls^{-1}) had the highest mean transport rate at 3.60 gs^{-1} ($\sigma = 1.92$) (Figure 4b). Abrupt changes in bedload transport rates occur around 1.14 Ls^{-1}, below which transport rates are consistently very low (< 0.40 gs^{-1}), and above which transport rates increase with discharge (Figure 4a). This threshold discharge of 1.14 Ls^{-1} serves as a useful tool for describing the shift in bedload transport rates from negligible to increasing with discharge. Although these experiments were not intended to investigate the role of hysteresis in gravel-bed braided rivers, separating the bedload transport data into rising and falling stages reveals no consistent hysteresis with changing discharge (Figure 4b).

Fractional Transport

Fractional transport rates were calculated as $q_{bi} = (p_i)q_b$, where *pi* is the proportion of each fraction (*i*) found in the bedload transported (q_b) for each run (Wilcock and McArdell, 1993). Across all discharges, bedload D_{10} ranged from 0.07- 0.57 mm, D_{50} ranged from 0.48- 1.41 mm, and D_{90} ranged from 1.15 to 3.57 mm (Figure 5). Overall, D_{10} was relatively constant across all discharges and hydrographs except for runs at the lowest discharge (0.7 Ls^{-1}), which had a mean D_{10} ($\bar{x}$ = 0.28 mm) lower than all the other discharges ($\bar{x}$ = 0.35 - 0.41 mm). While the mean D_{50} increased slightly with discharge from 0.65 to 1.07 mm it plateaued around a mean value of ~1 mm, which was close to the bulk D_{50} of 1.18 mm, above 1.35 Ls^{-1}. Of the three grain sizes investigated in detail, the D_{90} was the most responsive to increasing discharge and following the shape of the hydrograph, with no obvious or systematic hysteresis effect (Figure 5). The mean D_{90} increased from 1.56 mm at the lowest discharge to 2.9 mm under the peak discharge conditions, which was still lower than the mean bulk D_{90} of 3.52 mm.

For all three hydrographs, individual grain sizes were grouped into 6 classes and plotted as a mean percentage of the total bedload and as mean fractional transport rates for each discharge in Figure 6. At the lowest discharge (0.7 Ls^{-1}), grains smaller than 1 mm account for an average of 76 % of the total bedload, while less than 5 % of the bedload was grains larger than 2 mm. At higher discharges the GSD of the bedload is coarser, so that at the highest discharges, fine grains (<1 mm) account for ~ 47 % of the bedload and coarse grains (> 2 mm) account for ~ 20 % of the bedload. Grains between 1-2 mm, which includes the median of the subsurface (D_{50} = 1.18 mm), account for ~ 30 % of the total bedload, regardless of discharge. The only exception is the lowest discharge, for which grains of 1-2 mm only account for an average of 19 % of the total bedload. Only above 1.14 Ls^{-1} are the coarsest grains (>5.6 mm) detected in the bedload. Therefore, based on the discharge steps investigated during these experiments, 1.14 Ls^{-1} was the average threshold discharge between partial and selective mobility.

Comparison with Bed Material

While the D_{10}, D_{50}, and D_{90} varied within and between the hydrographs, even at the same discharges (Figure 5), plotting the GSD of all 117 bedload samples together indicates the steady shift in the grain size distributions as discharge increased (or decreased) between 0.7 Ls^{-1} to 2.1 Ls^{-1} (Figure 7). The complete distribution of the bulk subsurface was rarely reached in the bedload distributions and only at the channel-forming discharge of 2.1 Ls^{-1} does bedload approach equal mobility with regards the subsurface. This graph confirms that fine grains (i.e., D_{10}) are essentially fully mobilized regardless of discharge, while coarser grains transition from a state of immobility at low discharges, through partial mobilization towards full mobilization at the highest discharge.

Transition towards Equal Mobility

To investigate the changes in bed mobility with changing discharge, a *pi/fi* ratio was plotted in Figure 8, where *pi* is the frequency of grain size *i* in the total bedload and *fi* is the frequency of grain size *i* in the bulk distribution (Church and Hassan, 2002; Ferguson et al., 1992). Partial mobility is characterized by the curve dropping towards zero for large grain size while for selective mobility conditions, *pi/fi* decreases with grain size but remains above zero for large grain sizes. For 'true' equal mobility, *pi/fi* equals 1 for all grain sizes (Venditti et al., 2017). Figure 8 demonstrates that at higher discharge the distributions shift from a state of marginal partial mobility present at low discharge, through a state of selective mobility around 1.14 Ls^{-1} (i.e., where the coarsest fractions are 0 > *pi/fi* < 1, $\bar{x} = 0.018$, $\sigma = 0.037$), towards equal mobility, although strict true equal mobility was never reached. In terms of individual grain sizes, 1 mm (i.e., the approximate D_{50}) transitions from a *pi/fi* of 0.4 at 0.7 Ls^{-1} to 1.0 at the highest discharge. Also, fine grains (< 0.5 mm) are fully mobilized above a discharge of 0.83 Ls^{-1}. The coarsest grains (i.e., 5.6 mm) had a maximum *pi/fi* of 0.9, but even at the highest discharge the average *pi/fi* was only 0.27.

Using the ratio in the D_{90} of the surface (D_{90S}) and bedload (D_{90L}) as an indicator of bed material mobility, there was a decrease in the mobility ratio with mean dimensionless stream power (Ω^*) as defined by Lisle (1995):

$$\Omega^* = \frac{\rho Q S}{(\rho_s - \rho) g^{1/2} (D_{50})_b^{5/2}} \qquad 1$$

Where ρ is fluid density, Q is discharge, S is slope, D_{50} is mean grain size, ρ_s is sediment density, g is the acceleration due to gravity and b is the average wetted width (Figure 9a). This plot further demonstrates that true equal mobility generally not achieved with a minimum average mobility ratio of 1.2 (best fit power function with exponent -0.60). A similar relationship exists between the mobility ratio and bedload transport rate although the shape of the function shows stronger non-linearity (Figure 9b) than with dimensionless stream power.

Linkages to Morphological Active Depth and Active Width

DEMs of difference (DoDs) were used to estimate reach-averaged values of morphological change for each experimental run (Figure 10). Due to poor image quality, 3 DEMs were removed from analysis for a total of 113 DoDs across all three hydrographs. The DoDs demonstrate three emerging trends related to increasing discharge: 1) the maximum morphological active depth increased; 2) the active area (i.e., total area of erosion + total area of deposition) increased, and 3) the active areas were more continuous and contiguous along the channel.

Results for the reach-averaged morphological active depth and morphological active width can be seen in Figure 11. Across all discharges, the modal morphological active depth was approximately 2.5 mm (Figure 11a). For the three lowest discharges (0.7- 0.93 Ls^{-1}), the depth of scour was rarely (less than 20% of cases) greater than 3.5 mm (i.e., ~ D_{90} of the model subsurface). For the same three discharges, between 90- 99% of the active area had scour depths less than $2D_{90}$ (6 mm). At and above 1.14 Ls^{-1}, each of the morphological active depth distributions became increasingly positively skewed, reflecting the greater maximum depths of scour occurring with increasing discharge. At the peak discharge of 2.1 Ls^{-1}, only 70% of the recorded active depths are below 6 mm, and the greatest active depths recorded were greater than 25 mm, which is more than $20D_{50}$ and $7D_{90}$ of the model GSD.

Between 0.7 and 0.93 Ls^{-1}, the reach-average morphological active width was very small with averages between 0.02 - 0.03 m (s = 0.007 - 0.01) (Figure 11b). At and above 1.14 Ls^{-1}, the active width increased to an average of 0.06 m (σ = 0.036) and continued to increase with discharge to a mean of 0.38 m at the peak discharge of 2.1 Ls^{-1} (σ = 0.096). Therefore, both the morphological active depth and width had a similar discharge threshold as the transition from partial to selective mobility ~1.14 Ls^{-1} (Ω^*~70).

Plots of D_{10}, D_{50}, and D_{90} as a function of the bedload transport rate, reach-averaged morphological active depth, and the reach-averaged morphological active width are shown in Figure 12. Here the morphological active depth has been averaged for the entire 14 m study reach, so there is one mean observation for each experimental run. Both D_{50} and D_{90} have a positive power relationship with bedload transport rate, morphological active depth, and active width, but based on a least squares regression, D_{90} was more sensitive to changes in transport rate and morphology with R^2 values between 0.656-0.681 compared to the D_{50} (R^2 = 0.509 -0.604). As expected, D_{10} was not sensitive to either measure of morphological change (R^2 = 0.0837 -0.152), or bedload transport rate (R^2 = 0.150) because fine grains were fully mobilized under all discharge conditions (Figure 5). Furthermore, at very low discharges, when the bed was only partially mobile, the morphological active depth and active width are small, confirming that the finer tail of the gravel bed material moving over the bed results in little detectable morphological change. Separating rising and falling stage data shows no systematic hysteresis effect in the data (Figure 12).

To investigate differences between the three hydrographs, the initial bed hypsometry (see also Redolfi et al., 2018) and bed texture was plotted for each hydrograph (Figure 13 and see also Figure 3). The hypsometry analysis indicates that the initial topography of hydrographs A and C were nearly identical, but differed for B, although all three lie within the overall range of variability for the entire dataset. In terms of equivalent bed texture, the three hydrographs began with nearly identical distributions, all of which fall within the range of variability across all observations (Figure 13b). In addition to indicating that there was no apparent effect from running hydrograph A following a period of constant discharge evolution, these results highlight the inherent complexity and variability of braided river processes.

Discussion

In the physical model of a generic gravel-bed braided river, fractional transport rates, grain size distributions, and *pi/fi* ratios transition from a state of partial mobility to selective mobility at relatively low discharges and gradually approach near-equal mobility at peak channel-forming discharges and highest rates of morphological change.

In terms of individual grain sizes, the results showed that while D_{10} was essentially fully mobile across all experimental discharges, both D_{50} and D_{90} increased with discharge. D_{50} levelled off as it approached D_{50} of the model subsurface bulk sediment, indicating full mobilization of those fractions above discharges of 1.35 Ls^{-1}. D_{90} increased with discharge but did not level off, even at the channel-forming discharge of 2.1 Ls^{-1}, indicating only partial mobilization of coarse grains and therefore selective mobility of the bed. It is possible that with slightly higher discharges that the coarse grains would become more frequently fully mobilized. The results are similar to Ashworth et al. (1992) in a braided chute-bar structure, who found that while D_{50} was relatively constant, both spatially and temporally, D_{max} was sensitive to increasing flow strength through a single braided anabranch in the field. This is also consistent with earlier observations of Ashworth and Ferguson (1986, 1989) in a braided gravel outwash channel.

Looking at the complete GSD of the hydrographs demonstrated that the transition from partial mobility towards equal mobility was gradual and variable for each hydrograph. Since the peak flows modelled here were the same, differences in the GSDs likely reflect inherent variability in braiding processes and bedload response. In all cases, active braiding occurred for much of the hydrograph duration so that bed configuration and bed texture constantly varied. Local scour, channel shifting, bar development, and avulsion may all cause temporal variation in bedload transport rates and sources of bedload even at constant discharge (Ashmore, 1988; Bertoldi et al., 2009; Hoey, 1992; Peirce et al., 2018). For instance, there was a decrease in the D90 of hydrograph B (Figure 5) after the first four runs at peak discharge, possibly indicating a temporary decrease in the availability of coarse grain. This decrease in D_{90} in hydrograph B was also associated with ~23% decrease in both the morphological active depth and active width, highlighting the additional possible effect of morphological effects on particle mobility. During the subsequent hydrograph, hydrograph C, the morphology had shifted (Figure 3) through braiding processes, providing a fresh source of coarse grains.

These results follow previous research that suggests that there is a range of 'formative' or morphologically significant discharges over which bedload is transported depending on the morphological units (e.g., primary and secondary channels, bars etc.) being considered, which could also contribute to the overlapping GSDs for different discharges (Figure 7) (Mao and Surian, 2010; Surian et al., 2009). The differences in the three hydrographs highlight the importance of sampling multiple hydrographs, even over a similar morphology and small range of discharges, to capture the variability in GSDs and antecedent conditions of flow and channel morphology (Kociuba and Janicki, 2015; Powell et al., 2001b). It also points to the need for further model experiments to evaluate the effects of hydrograph duration and shape, as well as the related inherent variability in braiding morpho-dynamics.

The fractional transport analysis indicated the largest grain sizes (> 5.6 mm) only became transported above 1.14 Ls^{-1} ($\Omega^* = \sim70$) in the model. This discharge, which would represent approximately 8 m^3s^{-1} in the prototype river, is only ~ 50 % of the channel-forming (i.e., peak discharge) of 2.1 Ls^{-1} in the flume or ~15 m^3s^{-1} in the prototype. These results align with observations by Surian et al. (2009) and Mao and Surian (2010) who found that substantial morphological change and bed material mobilization occurred in the primary and secondary channels of gravel-bed rivers at discharges as low as 20-50% of bankfull. Together, these results demonstrate that some gravel-bed braided rivers may transition to selective mobility (i.e., the mobilization of coarse grains) at lower discharges than single-threaded gravel-bed rivers which may need discharges as high as 80 % of the bankfull discharge before gravel grains are mobilized, due to the need to mobilize the coarser grains in the surface layer (Ryan et al., 2002). In braiding rivers, the wide range of bed shear stress (Nicholas, 2000; Bertoldi et al., 2009) and local scour may produce high mobility at relatively low discharge in particular areas of the bed. Furthermore, as the threshold discharge between partial and selective mobility here was defined as approximately half of the channel-forming flow, the braided rivers modelled were dominated by selective mobility over almost all bed-mobilizing discharges. This is in contrast to the rather ubiquitous characterization of gravel-bed rivers as being only partially mobile due to a large population of immobile coarse grains that may only be mobilized at very high flows (Haschenburger and Wilcock, 2003; Venditti et al., 2017) falling into Church's (2006) category of "threshold channel 0.04+".

The relation between bed mobility and morphological active layer dimensions has not been thoroughly investigated for braiding rivers. In stable single-thread rivers, Wilcock and McArdell (1997) and Haschenburger and Wilcock (2003) found that full surface mobilization (i.e. selective mobility) of a gravel-bed was associated with active layer depth of ~$2D_{90}$. Similarly, Lisle (1995) found that the convergence of the bedload and bed material grain size was associated with large active layer thicknesses (e.g., 4-$12D_{84}$) and mobilization of large portions of the streambed area. The results here agree well with Wilcock and McArdell (1997) so that below 1.14 Ls^{-1}, when the bed is only partially mobilized and coarse grains are essentially immobile, the average morphological active depth was rarely (< 10 % of observations) greater than the $2D_{90}$ of 6 mm. Once 1.14 Ls^{-1} was reached, the morphological active depth increased with discharge so that scour depths greater than 25 mm ($7D_{90}$) were common above discharges of 1.65 Ls^{-1}, promoting full mobilization of the coarse bed material with increasing flow strength, similar to the results of Lisle (1995). Furthermore, the modal scour depth during bedload transport was close to 2.5 mm regardless of discharge. This suggests that transitions towards selective mobility and increases in bedload are not just due to increases in local maximum scour depth, but also the increase in the total morphologically active area of the bed (i.e., the morphological active width). This idea is supported with recent findings by Gardner et al. (2017) who found that confluence scours, which are commonly the locations of deepest scour, only occupied 21 % of the active area of a modelled braided gravel river bed.

From a visual inspection of the DoDs, the morphological active width expands and becomes more continuous along the channel with increasing flow strength (and see Peirce et al., 2018). Plots of the active width against discharge show a general threshold of 1.14 Ls^{-1}, below which the active with is narrow (< 3% of the wetted width) and relatively constant, and above which the active width expands linearly with increasing discharge to over 20% of the wetted width at high discharge. Overall, the results on morphological change indicate that areas of the bed do not remain immobile for long periods of time, so that the surface and subsurface are continuously being accessed and mobilized at relatively low discharges (> 1.14 Ls^{-1} in this case). Furthermore, increases in shear stress, while important for grain entrainment, may not be the only driver of bedload transport in morphologically-driven rivers like braided rivers. Again, a modal scour depth around 2.5 mm regardless of discharge suggests that it is not just an increase in shear stress at higher discharges but the increase in the area experiencing shear stresses above critical that is important (Bertoldi et al., 2009). This idea complements the findings of Haschenburger and Wilcock (2003) who described the transition of a gravel-bed river from partial to selective mobility as active areas of the bed expanded, and Ashmore & Sauks (2006) and Bertoldi et al. (2009) who found that braided rivers accommodate increases in discharge by increasing wetted width (and therefore morphological active width) with less change in mean water depth and mean velocity.

Finally, for the first time in braided river research, the relationship between morphological measurements of the morphological active depth and active width were compared to different grain size parameters for a large dataset. The results confirm that the movement of large grains, like D_{90}, are directly linked to changes in morphology in response to discharge forcing, specifically the vertical expansion of active depth and lateral expansion of the active width. This is consistent with greater braiding activity occurring at higher discharges during which lateral bank erosion, bar migration, bed scour at anabranch confluences, avulsion, and other braiding processes are more active (Wheaton et al., 2013). Also, the increased area of active layer turnover, as shown in the morphological change data, differs from the largely vertical exchange and limited bed scour observed in stable single channels and straight-walled flumes (Ashmore et al., 2018). These results suggest that in morphologically dynamic gravel-bed braided rivers, increases in bedload transport and the coarse grain mobilization above the threshold discharge is mediated by the availability of a wide range of sizes at the surface and subsurface as well as and the constant changes in the morphological active layer providing access to new sediment sources, laterally and vertically within the channel.

While these experiments provide interesting insights into the linkages between discharge, bedload grain size distributions and transport rates, and channel morphology in braided rivers, there are other considerations that should be investigated in the future. For example, while scale models have been vital for investigating grain size distributions and bed mobility relationships in gravel-bed rivers (e.g., Parker et al., 1982; Dietrich et al., 1989; Wilcock and McArdell, 1993), models often require simplifications that might not perfectly reflect the natural prototype. In this case, the grain size distribution of the model was truncated below 0.25 mm to avoid cohesion effects. Additional studies should investigate the role of fine grains on the GSD and bedload transport rates in braided rivers, as fines are known to enhance the mobilization of coarse grains and rates of bedload transport (Iseya and Ikeda, 1987; Venditti et al., 2010). Furthermore, given the possible impacts of different hydrograph structures on experimental outcomes, additional work should be done investigating more hydrograph structures as well as long-term (e.g., seasonal and annual) hydrologic regimes with a larger range of discharges. While the data show no clear hysteresis in bedload, morphological change which is consistent with recent hydrograph experiments of Redolfi et al., (2018), or bedload grain size, there is a possibility to examine the consistency and reasons for this effect in braiding rivers in more detail in the future. Finally, this research may be able to improve the numerical modelling of bedload transport and river morphodynamics rates in braided rivers (e.g., Williams et al., 2016b; Javernick et al., 2018). For instance, recent results from numerical morpho-dynamic modeling of braiding suggest that bed mobility may have a substantial effect on braiding morphology and dynamics (Sun et al., 2015) and data like those collected in these experiments could be used for validation and testing of these fundamental processes. On the basis of the current results this could be extended to understanding the role of surface coarsening (or lack of it) and bed material grain size distribution on morphological active layer dimensions and bedload grain size distributions in gravel braiding rivers.

Overall, the results point to a fundamental relationship between bed material mobility and morphological dynamics at varying discharge in some gravel braiding rivers. In order for significant morphological change to occur, as it does even at moderate discharges, much of the bed material needs to be mobilized. Therefore, the magnitude and frequency of morphological change are an indication of bed material mobility and without it active braiding would not occur (Ashmore et al., 2018). Specifically, the results of these experiments show that in braiding, full mobility of the median size occurs at moderate discharge but that large morphological change is associated with mobility of the coarse fractions. Limiting the mobility of the coarse fractions is then expected to reduce morphological dynamics and stabilize active braiding as shown recently by Mackenzie and Eaton (2017).

Conclusions

Physical model experiments were used to explore the evolution of grain size distributions and bed mobility in gravel-bed rivers in complex multi-threaded braided systems. Given the challenges to collecting simultaneous bedload transport and topographic data in the field, a physical model made it possible to measure bedload transport rates and changes in morphology over three event hydrographs similar to those found in a pro-glacial gravel-bed braided river. The model braided rivers transitioned from partial mobility to selective mobility at discharges above ~50% of peak discharge, and approached equal mobility at the highest (i.e., diurnal peak/channel-forming) discharges. This contrasts with stable, single-threaded gravel-bed rivers, which are normally dominated by partial mobility, even at bankfull discharges. The transition from partial mobility to selective mobility corresponded to the lower threshold for detectable morphological change and a substantial increase in bedload transport rates at approximately 50% of peak discharge, or dimensionless stream power (Lisle, 1995) of 70. Morphological change and bed material transport and mobility are closely connected as discharge changes. With increasing (decreasing) discharge the morphological active layer progressively expands (contracts) both vertically and laterally, with active layer depth reaching maximum values up to 9 times D_{90}. The highest particle mobility states are associated with the highest discharge and the most intense rates and greatest extents of morphological change; the most active braiding occurs when coarse grains are mobilized and vice versa.

These results contribute to the overall understanding of braided river morphodynamics by demonstrating the strong linkages between the thresholds for detectable morphological change, bedload transport rates, and coarse grain mobilization. Until now, there have been no studies, in the field or flume, that have been able to link discharge variation and channel morphology with grain size distributions in gravel-bed braided rivers in this way. In turn, these results will have implications for assessing and modelling bedload transport and channel stability in braiding rivers, and show the importance of extending analyses of bedload dynamics to a wider range of channel types..

Acknowledgements

This research was supported by a Natural Sciences and Engineering Research Council Discovery Grant to P. Ashmore and flume construction was supported by the Canada Foundation for Innovation and Newalta Resources Inc. Additional funding support was provided by the Vanier Canada Graduate Scholarship awarded to S. Peirce. Thank you to everyone who assisted with the experiments, especially Lara Middleton and Danielle Barr.

References

Ashmore P. 1988. Bed load transport in braided gravel-bed stream models. Earth Surface Processes and Landforms **13**: 677–695.DOI: 10.1002/esp.3290130803

Ashmore P. 2013. Morphology and Dynamics of Braided Rivers. In Treatise on Geomorphology , Shroder J and Wohl E (eds). Elsevier: San Diego; 289–312.

Ashmore P, Bertoldi W, Tobias Gardner J, Gardner JT. 2011. Active width of gravel-bed braided rivers. Earth Surface Processes and Landforms **36**: 1510–1521.DOI: 10.1002/esp.2182

Ashmore P, Church M. 1998. Sediment transport and river morphology: a paradigm for study. In Gravel-Bed Rivers in the Environment , . 115–148.

Ashmore P, Peirce S, Leduc P. 2018. Expanding the “Active Layer”: Discussion of Church and Haschenburger (2017) What is the “Active Layer”? Water Resources Research 53, 5-10, Doi:10.1002/2016WR019675. Water Resources Research **54**: 1425–1427.DOI: 10.1002/2017WR022438

Ashmore P, Sauks E. 2006. Prediction of discharge from water surface width in a braided river with implications for at-a-station hydraulic geometry. Water Resources Research **42**: 1–11.DOI: 10.1029/2005WR003993

Ashmore PE. 1982. Laboratory modelling of gravel braided stream morphology. Earth Surface Processes and Landforms **7**: 201–225.DOI: 10.1002/esp.3290070301

Ashworth PJ, Ferguson RI. 1986. Interrelationships of Channel Processes, Changes and Sediments in a Proglacial Braided River. Geografiska Annaler. Series A, Physical Geography **68**: 361.DOI: 10.2307/521527

Ashworth PJ, Ferguson RI. 1989. Size-selective entrainment of bed load in gravel bed streams. Water Resources Research **25**: 627–634.DOI: 10.1029/WR025i004p00627

Ashworth PJ, Ferguson RI, Ashmore P, Paola C, Powell DM, Prestegaards KL, Prestegaard KL, Prestegaards KL. 1992. Measurements in a Braided River chute and lobe: 2. Sorting of bed load during entrainment, transport, and deposition. Water Resources Research **28**: 1887–1896.DOI: 10.1029/92WR00702

Bertoldi W, Ashmore P, Tubino M. 2009. A method for estimating the mean bed load flux in braided rivers. Geomorphology **103**: 330–340.DOI: 10.1016/j.geomorph.2008.06.014

Bluck BJ. 1979. Structure of coarse grained braided stream alluvium. Earth and Environmental Science Transactions of the Royal Society of Edinburgh **70**: 181–221.

Brasington J, Rumsby BT, Mcvey RA. 2000. Monitoring and modelling morphological change in a braided gravel-bed river using high resolution GPS-based survey. Earth Surface Processes and Landforms **25**: 973–990.DOI: 10.1002/1096-9837(200008)25

Bunte K, Abt SR. 2001. Summary for Policymakers. In Climate Change 2013 - The Physical Science Basis , Intergovernmental Panel on Climate Change (ed). Cambridge University Press: Cambridge; 1–30.

Carbonneau PE, Bergeron N, Lane SN. 2005. Automated grain size measurements from airborne remote sensing for long profile measurements of fluvial grain sizes. Water Resources Research **41**: 1–9.DOI: 10.1029/2005WR003994

Carson MA, Griffiths GA. 1987. Bedload Transport in Gravel Channels. Journal of Hydrology New Zealand **26**

Chew L., Ashmore P. 2001. Channel adjustment and a test of rational regime theory in a proglacial braided stream. Geomorphology **37**: 43–63.DOI: 10.1016/S0169-555X(00)00062-3

Church M. 2006. Bed Material Transport and the Morphology of Alluvial River Channels. Annual Review of Earth and Planetary Sciences **34**: 325–354.DOI: 10.1146/annurev.earth.33.092203.122721

Church M, Haschenburger JK. 2017. What is the “active layer”? Water Resources Research **53**: 5–10.DOI: 10.1002/2016WR019675

Church M, Hassan MA. 2002. Mobility of bed material in Harris Creek. Water Resources Research **38**: 19-1-19–12.DOI: 10.1029/2001WR000753

Davies T. 1987. Problems of bed load transport in braided gravel-bed rivers. In Sediment Transfer in Gravel-Bed Rivers , Thorne CR, Bathurst JC, and Hey RD (eds).

John Wiley & Sons; 793–811.

Dietrich WE, Kirchner JW, Ikeda H, Iseya F. 1989. Sediment supply and the development of the coarse surface layer in gravel-bedded rivers. Nature **340**: 215–217.DOI: 10.1038/340215a0

Egozi R, Ashmore P. 2008. Defining and measuring braiding intensity. Earth Surface Processes and Landforms **33**: 2121–2138.DOI: 10.1002/esp.1658

Ferguson RI. 1987. Hydraulic and Sedimnetary Controls of Channel Pattern. In River channels , Richards K (ed). Basil Blackwell; 129–158.

Ferguson RI, Ashmore P, Ashworth PJ, Paola C, Prestegaard KL. 1992. Measurements in a Braided River chute and lobe: 1. Flow pattern, sediment transport, and channel change. Water Resources Research **28**: 1877–1886.DOI: 10.1029/92WR00700

Gardner JT, Ashmore P. 2011a. Geometry and grain-size characteristics of the basal surface of a braided river deposit. Geology **39**: 247–250.DOI: 10.1130/G31639.1

Gardner JT, Ashmore P. 2011b. Geometry and grain-size characteristics of the basal surface of a braided river deposit. Geology **39**: 247–250.DOI: 10.1130/G31639.1

Gardner T, Ashmore P, Leduc P. 2017. Morpho-sedimentary characteristics of proximal gravel braided river deposits in a Froude-scaled physical model. Sedimentology **38**: 42–49.DOI: 10.1111/sed.12409

Guerit L, Barrier L, Narteau C, Métivier F, Liu Y, Lajeunesse E, Gayer E, Meunier P, Malverti L, Ye B. 2014. The grain-size patchiness of braided gravel-bed streams - Example of the Urumqi River (northeast Tian Shan, China). Advances in Geosciences **37**: 27–39.DOI: 10.5194/adgeo-37-27-2014

Haschenburger JK, Wilcock PR. 2003. Partial transport in a natural gravel bed channel.

Water Resources Research **39**: 1–9.DOI: 10.1029/2002WR001532

Hoey T. 1992. Temporal variations in bedload transport rates and sediment storage in gravel-bed rivers. Progress in Physical Geography **16**: 319–338.DOI: 10.1177/030913339201600303

Hoey TB, Sutherland AJ. 1991. Channel morphology and bedload pulses in braided rivers: a laboratory study. Earth Surface Processes and Landforms **16**: 447–462.DOI: 10.1002/esp.3290160506

Iseya F, Ikeda H. 1987. Pulsations in Bedload Transport Rates Induced by a Longitudinal Sediment Sorting: A Flume Study Using Sand and Gravel Mixtures. Geografiska Annaler. Series A, Physical Geography **69**: 15.DOI: 10.2307/521363

Javernick L, Redolfi M, Bertoldi W. 2018. Evaluation of a numerical model's ability to predict bed load transport observed in braided river experiments. Advances in Water Resources **115**: 207–218.DOI: 10.1016/j.advwatres.2018.03.012

Kasprak A, Wheaton JM, Ashmore P, Hensleigh JW, Peirce S. 2015. The relationship between particle travel distance and channel morphology: Results from physical models of braided rivers. Journal of Geophysical Research: Earth Surface **120**: 55–74.DOI: 10.1002/2014JF003310

Kociuba W, Janicki G. 2015. Changeability of Movable Bed-Surface Particles in Natural, Gravel-Bed Channels and Its Relation to Bedload Grain Size Distribution (Scott River, Svalbard). Geografiska Annaler: Series A, Physical Geography **97**: 507–521.DOI: 10.1111/geoa.12090

Laronne J. B, Reid I, Yitshak Y, Frostick LE. 1994. The non-layering of gravel streambeds under ephemeral flood regimes. Journal of Hydrology **159**: 353–363.DOI:

10.1016/0022-1694(94)90266-6

Laronne J. B, Reid L. 1993. Very high rates of bedload sediment transport by ephemeral desert rivers. Nature **366**: 148–150.DOI: 10.1038/366148a0

Leduc P, Ashmore P, Gardner JT. 2015. Grain sorting in the morphological active layer of a braided river physical model. Earth Surface Dynamics **3**: 577–585.DOI: 10.5194/esurf-3-577-2015

Lisle TE. 1995. Particle size variations between bed load and bed material in natural gravel bed channels. Water Resources Research **31**: 1107–1118.

Lisle TE, Nelson JM, Pitlick J, Madej MA, Barkett BL. 2000. Variability of bed mobility in natural, gravel-bed channels and adjustments to sediment load at local and reach scales. Water Resources Research **36**: 3743–3755.DOI: 10.1029/2000WR900238

Lugo GAG, Bertoldi W, Henshaw AJ, Gurnell AM. 2015. The effect of lateral confinement on gravel bed river morphology. Water Resources Research **51**: 7145–7158.DOI: 10.1002/2015WR017081

MacKenzie LG, Eaton BC. 2017. Large grains matter: contrasting bed stability and morphodynamics during two nearly identical experiments. Earth Surface Processes and Landforms **42**: 1287–1295.DOI: 10.1002/esp.4122

Mao L, Surian N. 2010. Observations on sediment mobility in a large gravel-bed river. Geomorphology **114**: 326–337.DOI: 10.1016/j.geomorph.2009.07.015

Morgan JA, Brogan DJ, Nelson PA. 2016. Application of Structure-from-Motion photogrammetry in laboratory flumes. Geomorphology **276**: 125–143.DOI: 10.1016/j.geomorph.2016.10.021

Mueller ER, Pitlick J. 2013. Sediment supply and channel morphology in mountain river systems: 1. Relative importance of lithology, topography, and climate. Journal of Geophysical Research: Earth Surface **118**: 2325–2342.DOI: 10.1002/2013JF002843

Mueller ER, Pitlick J. 2014. Sediment supply and channel morphology in mountain river systems: 2. Single thread to braided transitions. Journal of Geophysical Research: Earth Surface **119**: 1516–1541.DOI: 10.1002/2013JF003045

Parker G. 2008. Transport of Gravel and Sediment Mixtures. In Sedimentation Engineering: Processes, Measurements, Modeling, and Practice , Garcia M (ed). American Society of Civil Engineers: Reston, VA; 165–252.

Parker G, Dhamotharan S, Stefan H. 1982. Model experiments on mobile, paved gravel bed streams. Water Resources Research **18**: 1395–1408.DOI: 10.1029/WR018i005p01395

Parker G, Klingeman PC. 1982. On why gravel bed streams are paved. Water Resources Research **18**: 1409–1423.DOI: 10.1029/WR018i005p01409

Parker G, Toro-Escobar CM. 2002. Equal mobility of gravel in streams: The remains of the day. Water Resources Research **38**: 46-1-46–8.DOI: 10.1029/2001WR000669

Peirce S, Ashmore P, Leduc P. 2018. The Variability in the Morphological Active Width: Results from Physical Models of Gravel-Bed Braided Rivers. Earth Surface Processes and Landforms : 1–38. DOI: 10.1002/esp.4400

Piegay H, Grant G, Nakamura F, Trustrum N. 2006. Braided River Management: from Assessment of River Behaviour to Improved Sustainable Development. In Braided Rivers: Process, Deposits, Ecology and Management , . Blackwell Publishing Ltd.: Oxford, UK; 257–275.

Powell DM, Ashworth PJ. 1995. Spatial Pattern of Flow Competence and Bed Load

Transport in a Divided Gravel Bed River. Water Resources Research **31**: 741–752.DOI: 10.1029/94WR02273

Powell DM, Reid I, Laronne B. 2001a. Evolution of bed load grain size distribution with increasing flow strength and the effect of flow duration on the caliber of bed load sediment yield in ephemeral gravel bed rivers. Water Resources Research **37**: 1463–1474.

Powell DM, Reid I, Laronne J. BB. 2001b. Evolution of bed load grain size distribution with increasing flow strength and the effect of flow duration on the caliber of bed load sediment yield in ephemeral gravel bed rivers. Water Resources Research **37**: 1463–1474.DOI: 10.1029/2000WR900342

Recking A, Piton G, Vazquez-Tarrio D, Parker G. 2016. Quantifying the Morphological Print of Bedload Transport. Earth Surface Processes and Landforms **41**: 809–822.DOI: 10.1002/esp.3869

Redolfi M, Bertoldi W, Tubino M, Welber M. 2018. Bed Load Variability and Morphology of Gravel Bed Rivers Subject to Unsteady Flow: A Laboratory Investigation. Water Resources Research **54**: 842–862.DOI: 10.1002/2017WR021143

Ryan SE, Porth LS, Troendle CA. 2002. Defining phases of bedload transport using piecewise regression. Earth Surface Processes and Landforms **27**: 971–990.DOI: 10.1002/esp.387

Smith ND. 1974. Sedimentology and Bar Formation in the Upper Kicking Horse River, a Braided Outwash Stream. The Journal of Geology **82**: 205–223.

Sun J, Lin B, Yang H. 2015. Development and application of a braided river model with non-uniform sediment transport. Advances in Water Resources **81**: 62–74.DOI:

10.1016/j.advwatres.2014.12.012

Surian N, Mao L, Giacomin M, Ziliani L. 2009. Morphological effects of different channel- forming discharges in a gravel-bed river. Earth Surface Processes and Landforms **34**: 1093–1107.DOI: 10.1002/esp.1798

Venditti JG, Dietrich WE, Nelson PA, Wydzga MA, Fadde J, Sklar L. 2010. Mobilization of coarse surface layers in gravel-bedded rivers by finer gravel bed load. Water Resources Research **46**: 1–10.DOI: 10.1029/2009WR008329

Venditti JG, Nelson PA, Bradley RW, Haught D, Gitto AB. 2017. Bedforms, Structures, Patches, and Sediment Supply in Gravel-Bed Rivers. In Gravel-Bed Rivers , . John Wiley & Sons, Ltd: Chichester, UK; 439–466.

Warburton J, Davies T. 1994. Variability of bedload transport and channel morphology in a braided river hydraulic model. Earth Surface Processes and Landforms **19**: 403–421.DOI: 10.1002/esp.3290190503

Wheaton JM, Brasington J, Darby SE, Kasprak A, Sear DA, Vericat D. 2013. Morphodynamic signatures of braiding mechanisms as expressed through change in sediment storage in a gravel-bed river. Journal of Geophysical Research: Earth Surface **118**: 759–779.DOI: 10.1002/jgrf.20060

Wilcock PR, McArdell BW. 1993. Surface-based fractional transport rates: Mobilization thresholds and partial transport of a sand-gravel sediment. Water Resources Research **29**: 1297–1312.DOI: 10.1029/92WR02748

Wilcock PR, McArdell BW. 1997a. Partial transport of a sand/gravel sediment. Water Resources Research **33**: 235–245.DOI: 10.1029/96WR02672

Wilcock PR, McArdell BW. 1997b. Partial transport of a sand / gravel sediment flume.

Water Resources Research **33**: 235–245.

Williams RD, Brasington J, Hicks DM. 2016a. Numerical Modelling of Braided River Morphodynamics: Review and Future Challenges. Geography Compass **10**: 102–127.DOI: 10.1111/gec3.12260

Williams RD, Measures R, Hicks DM, Brasington J. 2016b. Assessment of a numerical model to reproduce event-scale erosion and deposition distributions in a braided river. Water Resources Research **52**: 6621–6642.DOI: 10.1002/2015WR018491

Williams RD, Rennie CD, Brasington J, Hicks DM, Vericat D. 2015a. Linking the spatial distribution of bed load transport to morphological change during high-flow events in a shallow braided river. Journal of Geophysical Research: Earth Surface **120**: 604–622.DOI: 10.1002/2014JF003346

Williams RD, Rennie CD, Brasington J, Hicks DM, Vericat DD. 2015b. Linking the spatial distribution of bed load transport to morphological change during high-flow events in a shallow braided river. Journal of Geophysical Research: Earth Surface **120**: 604–622.DOI: 10.1002/2014JF003346

Young WJ, Warburton J. 1996. Principles and practice of hydraulic modelling of braided gravel-bed rivers. Journal of Hydrology New Zealand **35**: 175–198.DOI: 10.1016/S0301-9322(97)80098-5

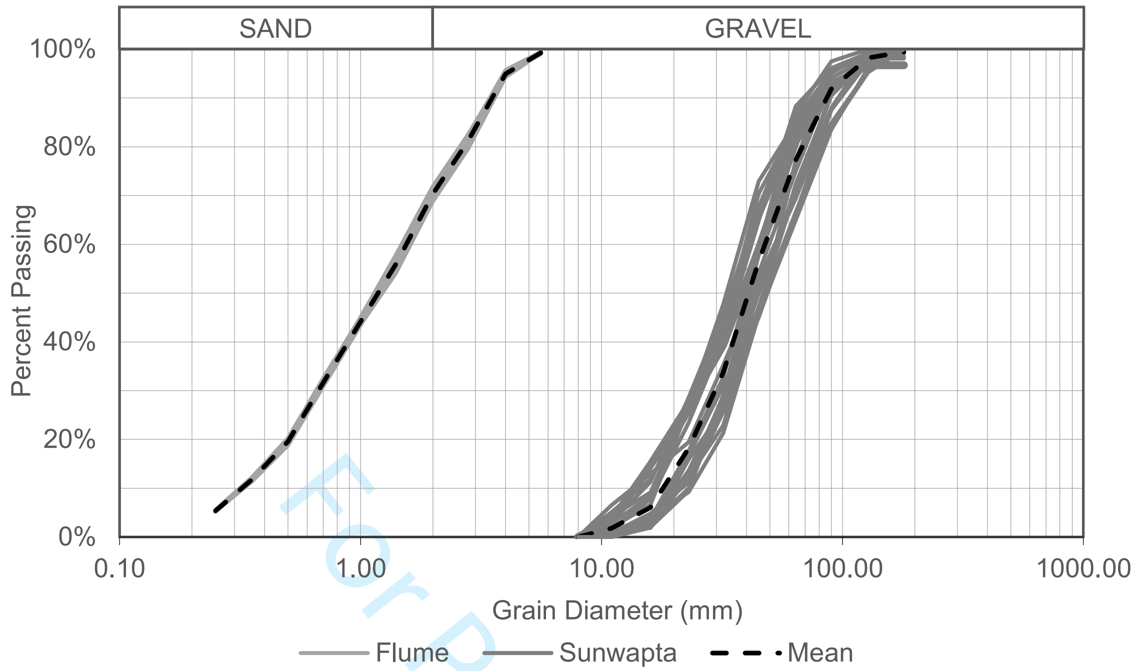
SAND
GRAVEL
100%
80%
60%
40%
20%
0%
Percent Passing
0.10
1.00
10.00
100.00
1000.00
Grain Diameter (mm)
Flume
Sunwapta
Mean

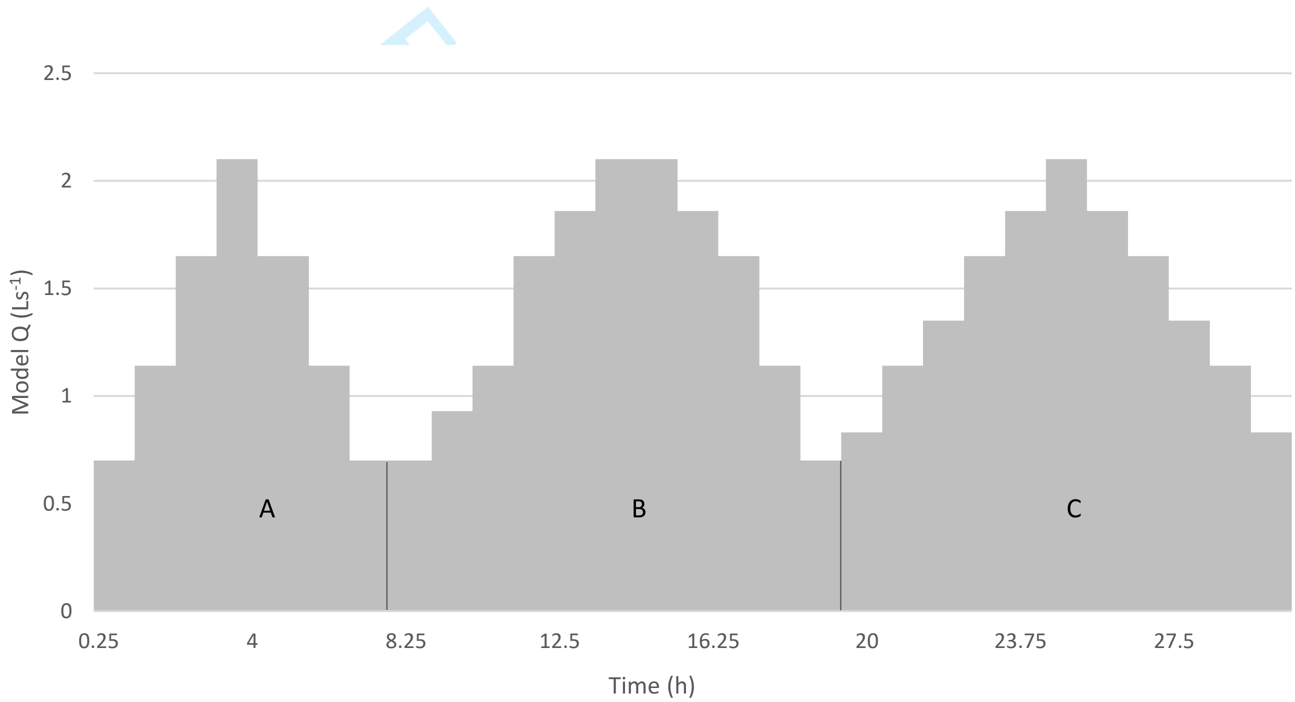
2.5
2
1.5
1
0.5
0
Model Q (Ls-1)
A
B
C
0.25
4
8.25
12.5
16.25
20
23.75
27.5
Time (h)

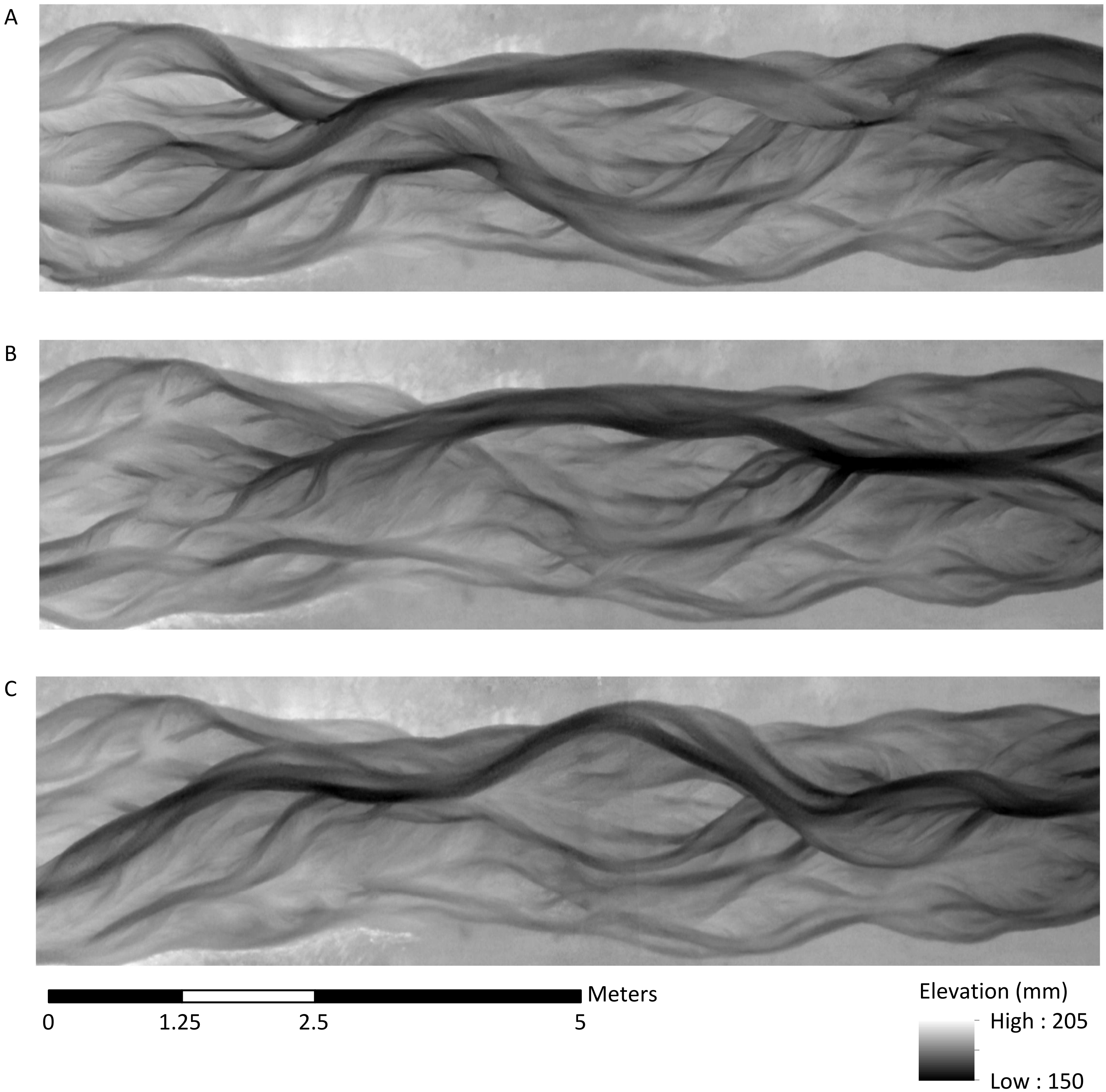
A
B
C
Meters
0
1.25
2.5
5
Elevation (mm)
High : 205
Low : 150

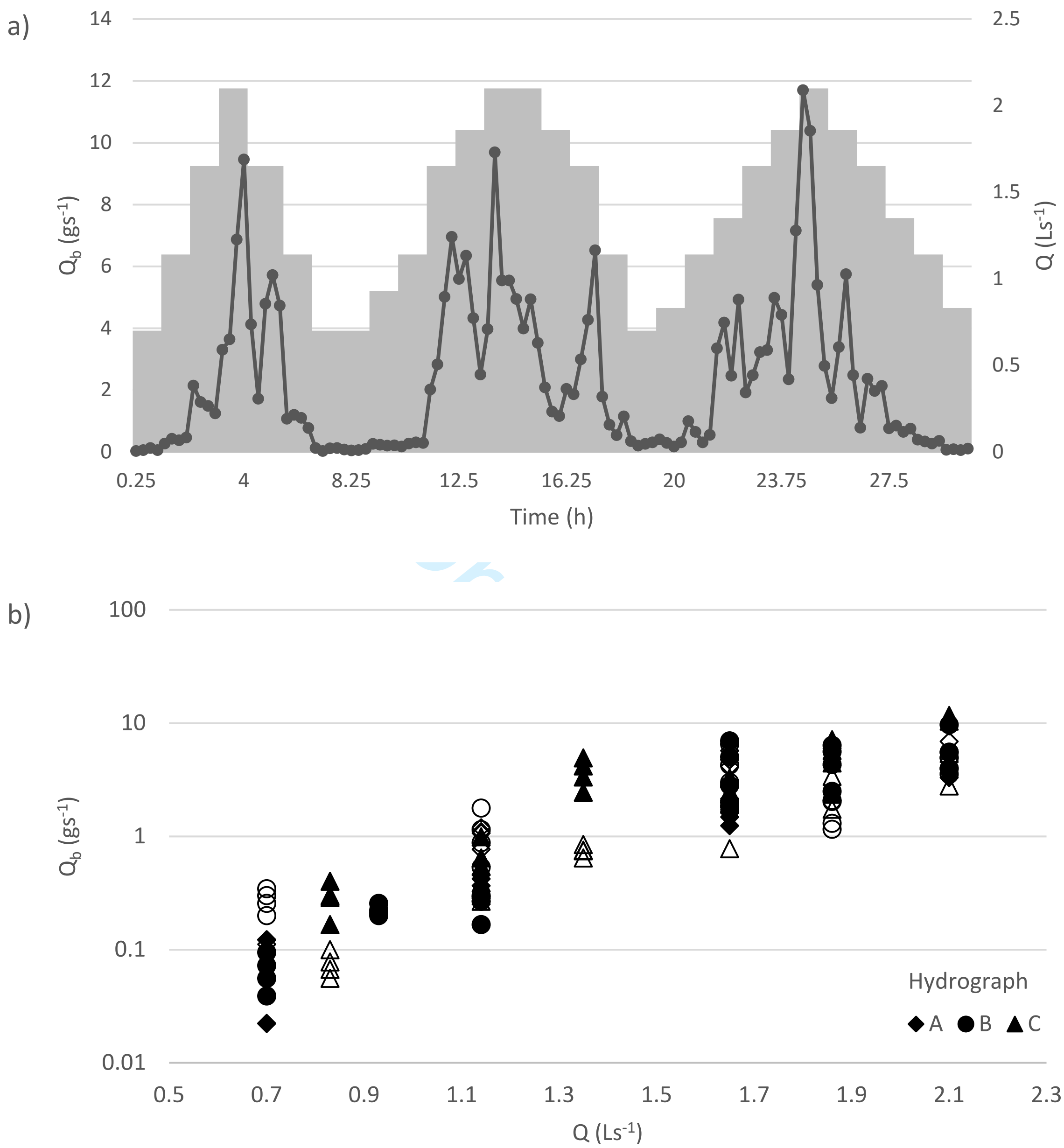
a)
14
12
10
8
6
4
2
0
Qb (gs-1)
2.5
2
1.5
1
0.5
0
Q (Ls-1)
0.25
4
8.25
12.5
16.25
20
23.75
27.5
Time (h)
b)
100
10
1
0.1
0.01
Qb (gs-1)
0.5
0.7
0.9
1.1
1.3
1.5
1.7
1.9
2.1
2.3
Q (Ls-1)
Hydrograph
A
B
C

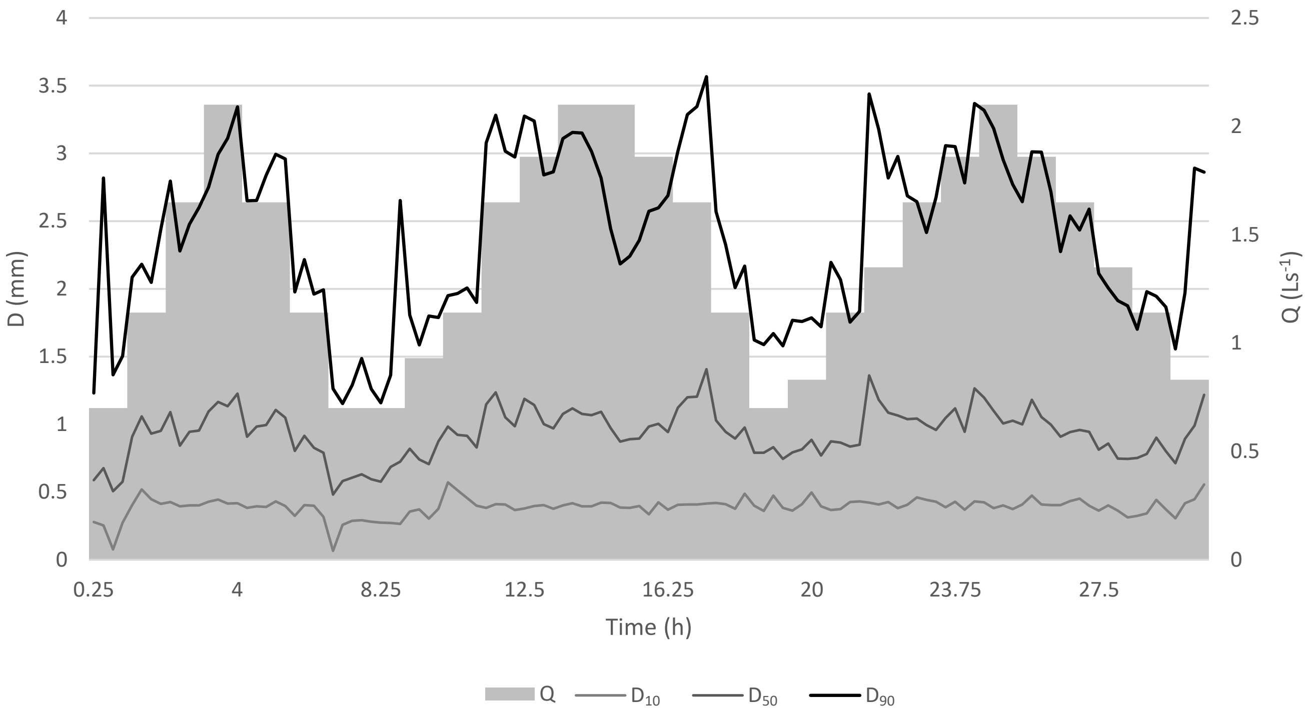
4
3.5
3
2.5
2
1.5
1
0.5
0
D (mm)
2.5
2
1.5
1
0.5
0
Q (Ls-1)
0.25
4
8.25
12.5
16.25
20
23.75
27.5
Time (h)
Q
D10
D50
D90

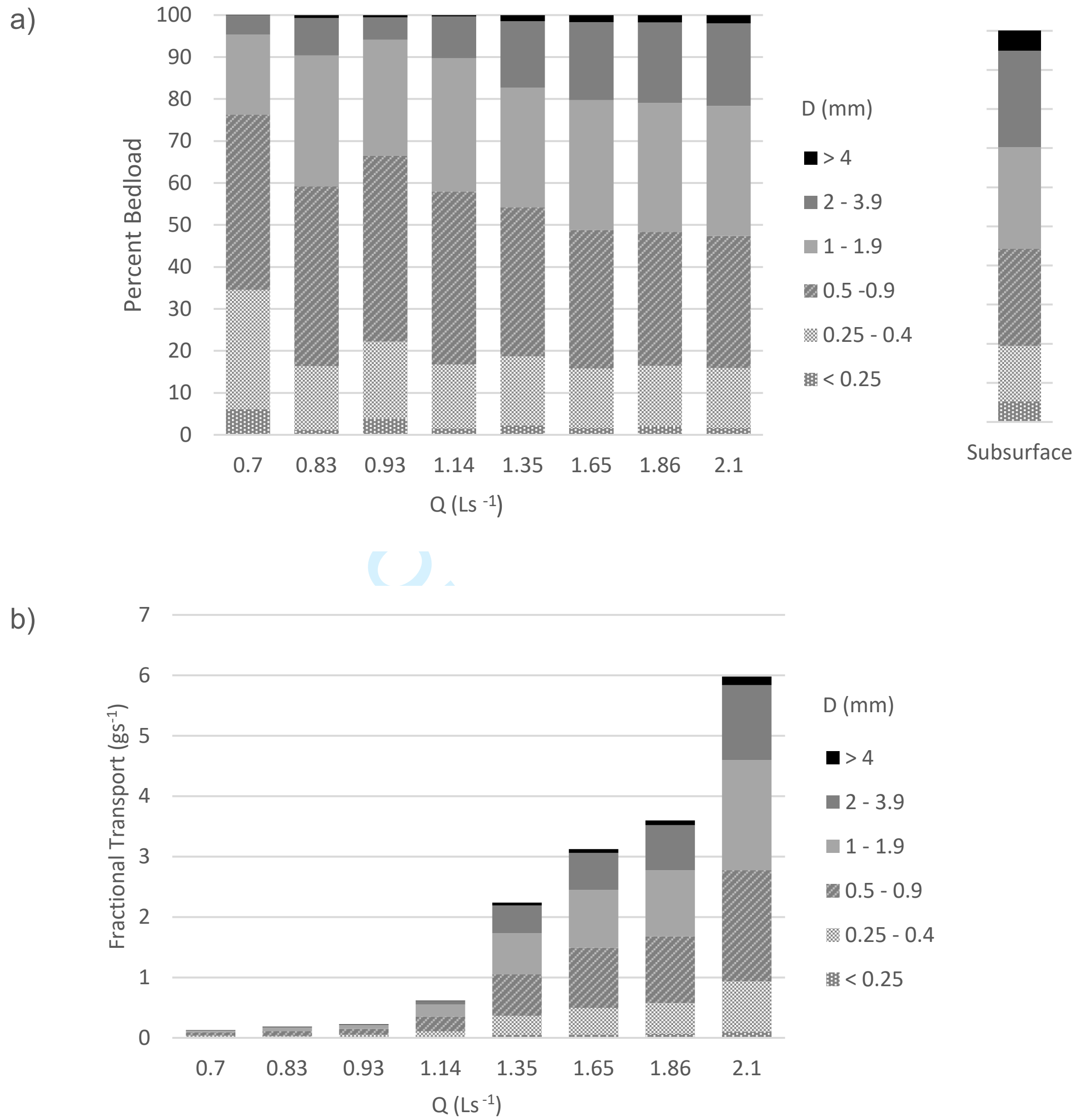
a)
100
90
80
70
60
50
40
30
20
10
0
Percent Bedload
0.7
0.83
0.93
1.14
1.35
1.65
1.86
2.1
Q (Ls -1)
D (mm)
> 4
2 - 3.9
1 - 1.9
0.5 -0.9
0.25 - 0.4
< 0.25
Subsurface
b)
7
6
5
4
3
2
1
0
Fractional Transport (gs-1)
0.7
0.83
0.93
1.14
1.35
1.65
1.86
2.1
Q (Ls -1)
D (mm)
> 4
2 - 3.9
1 - 1.9
0.5 - 0.9
0.25 - 0.4
< 0.25

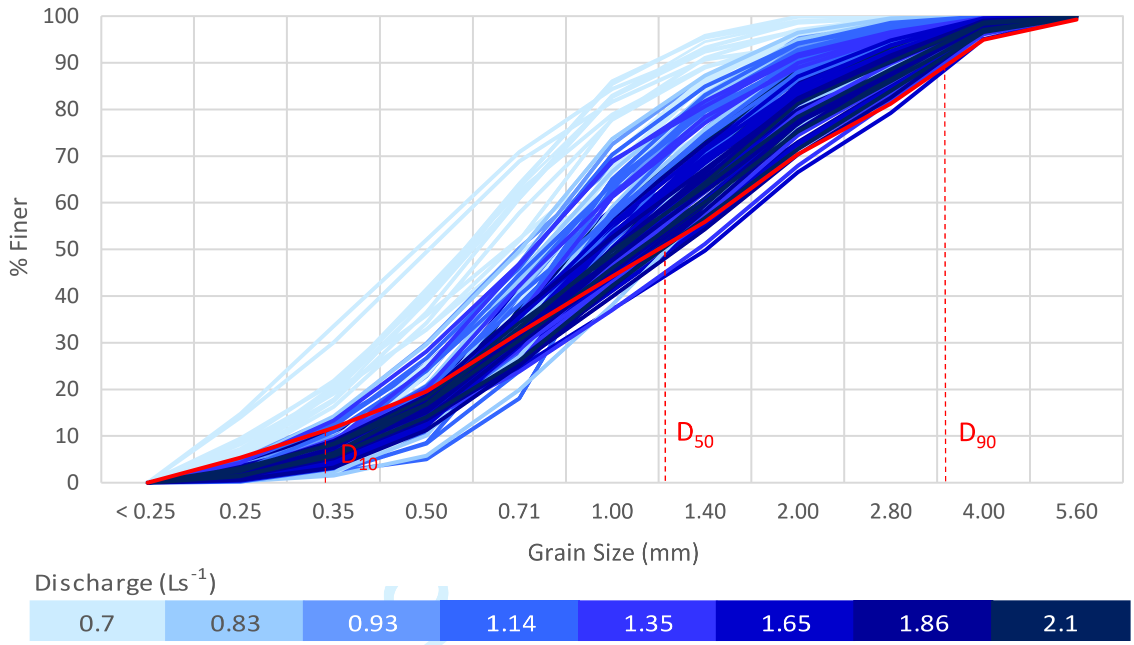

100
90
80
70
60
50
40
30
20
10
0
% Finer
D10
D50
D90
< 0.25
0.25
0.35
0.50
0.71
1.00
1.40
2.00
2.80
4.00
5.60
Grain Size (mm)
Discharge (Ls-1)
0.7
0.83
0.93
1.14
1.35
1.65
1.86
2.1

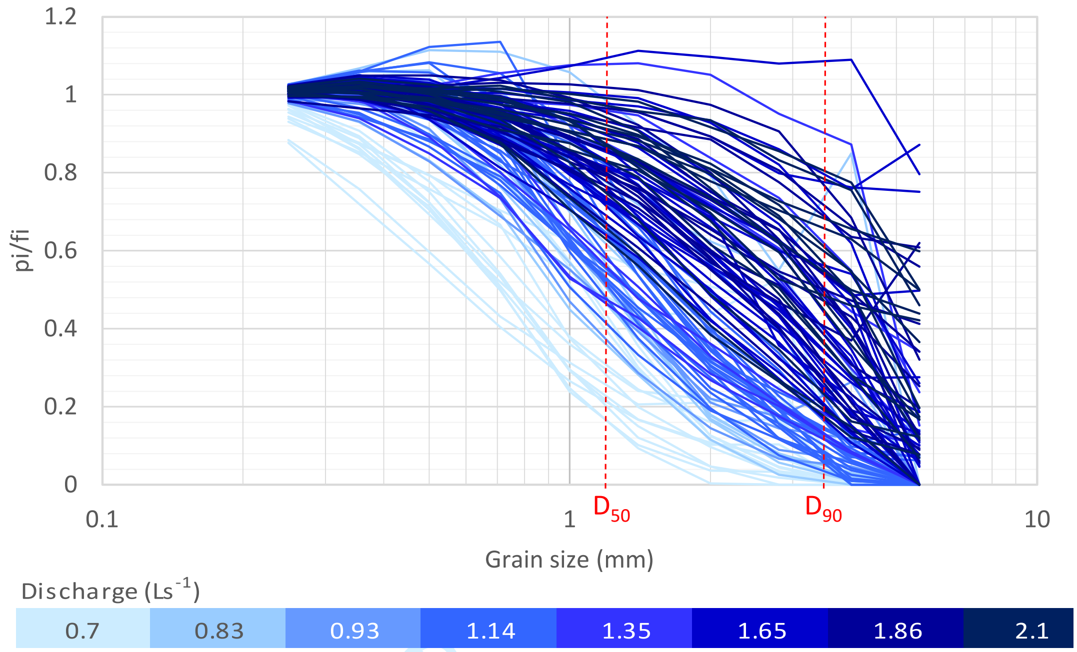

1.2
1
0.8
0.6
0.4
0.2
0
pi/fi
0.1
1
10
D50
D90
Grain size (mm)
Discharge (Ls-1)
0.7
0.83
0.93
1.14
1.35
1.65
1.86
2.1

a)

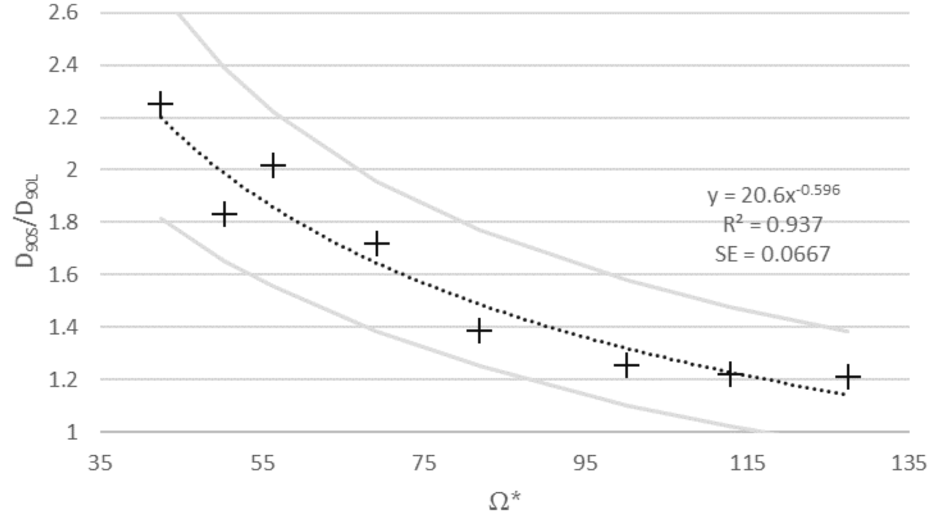
2.6
2.4
2.2
2
1.8
1.6
1.4
1.2
1
35
55
75
95
115
135
D_{90S}/D_{90L}
Ω*
y = 20.6x^-0.596
R² = 0.937
SE = 0.0667

b)

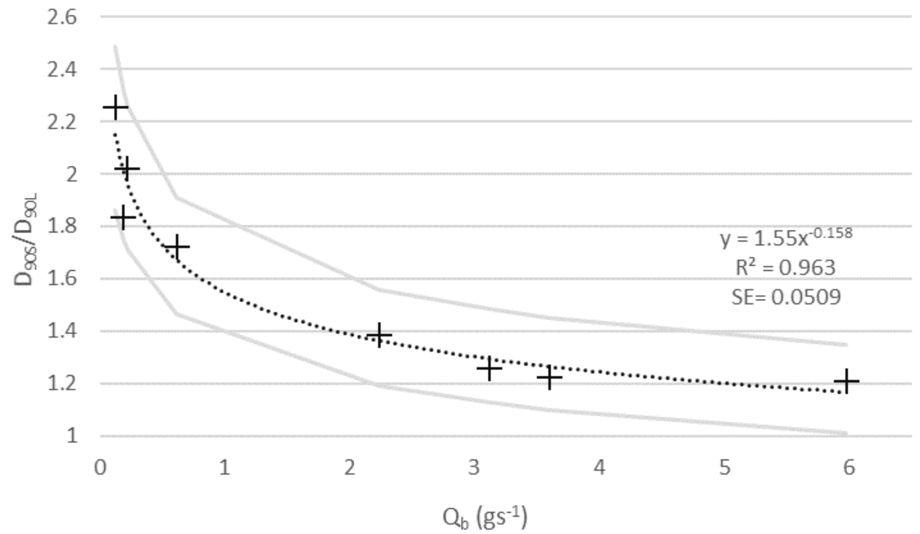
2.6
2.4
2.2
2
1.8
1.6
1.4
1.2
1
0
1
2
3
4
5
6
D_{90S}/D_{90L}
Q_b (gs^-1)
y = 1.55x^-0.158
R² = 0.963
SE= 0.0509

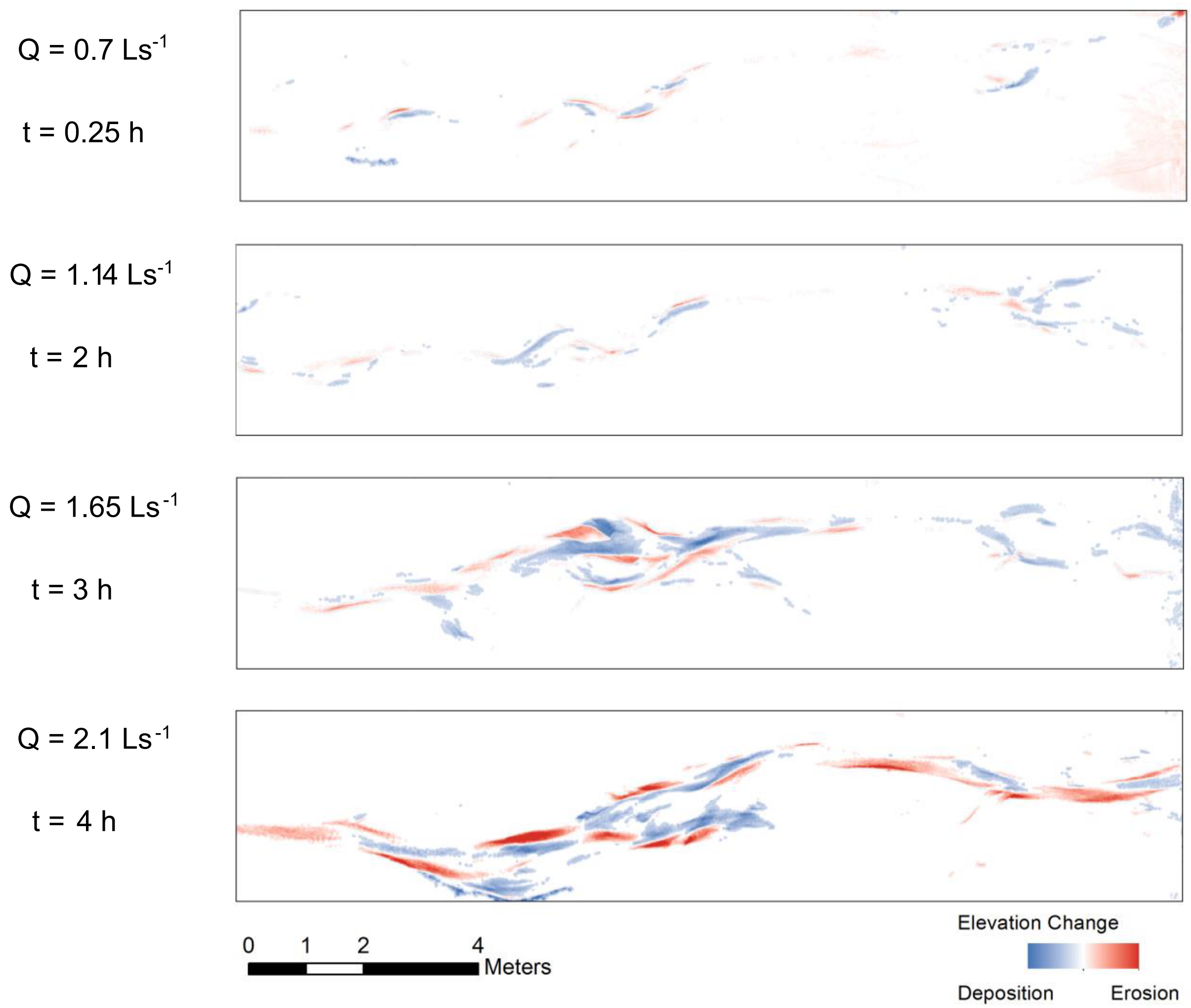
Q = 0.7 Ls-1
t = 0.25 h
Q = 1.14 Ls-1
t = 2 h
Q = 1.65 Ls-1
t = 3 h
Q = 2.1 Ls-1
t = 4 h
0 1 2 4
Meters
Elevation Change
Deposition
Erosion

a)

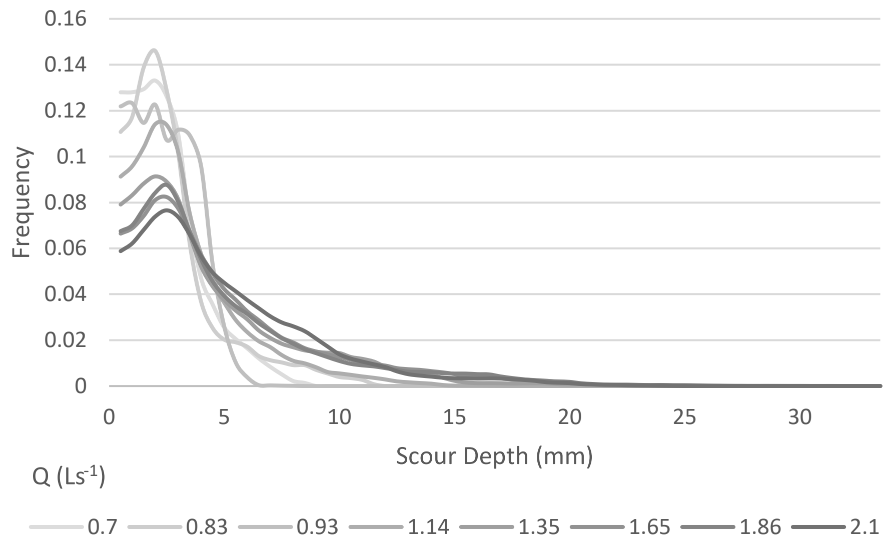
Frequency
0.16
0.14
0.12
0.1
0.08
0.06
0.04
0.02
0
0
5
10
15
20
25
30
Scour Depth (mm)
Q (Ls-1)
0.7
0.83
0.93
1.14
1.35
1.65
1.86
2.1

b)

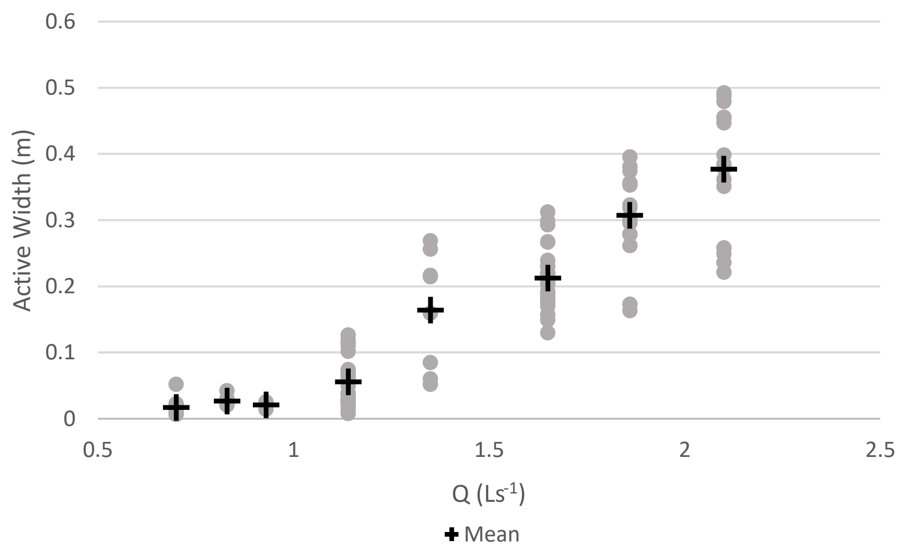
Active Width (m)
0.6
0.5
0.4
0.3
0.2
0.1
0
0.5
1
1.5
2
2.5
Q (Ls-1)
Mean

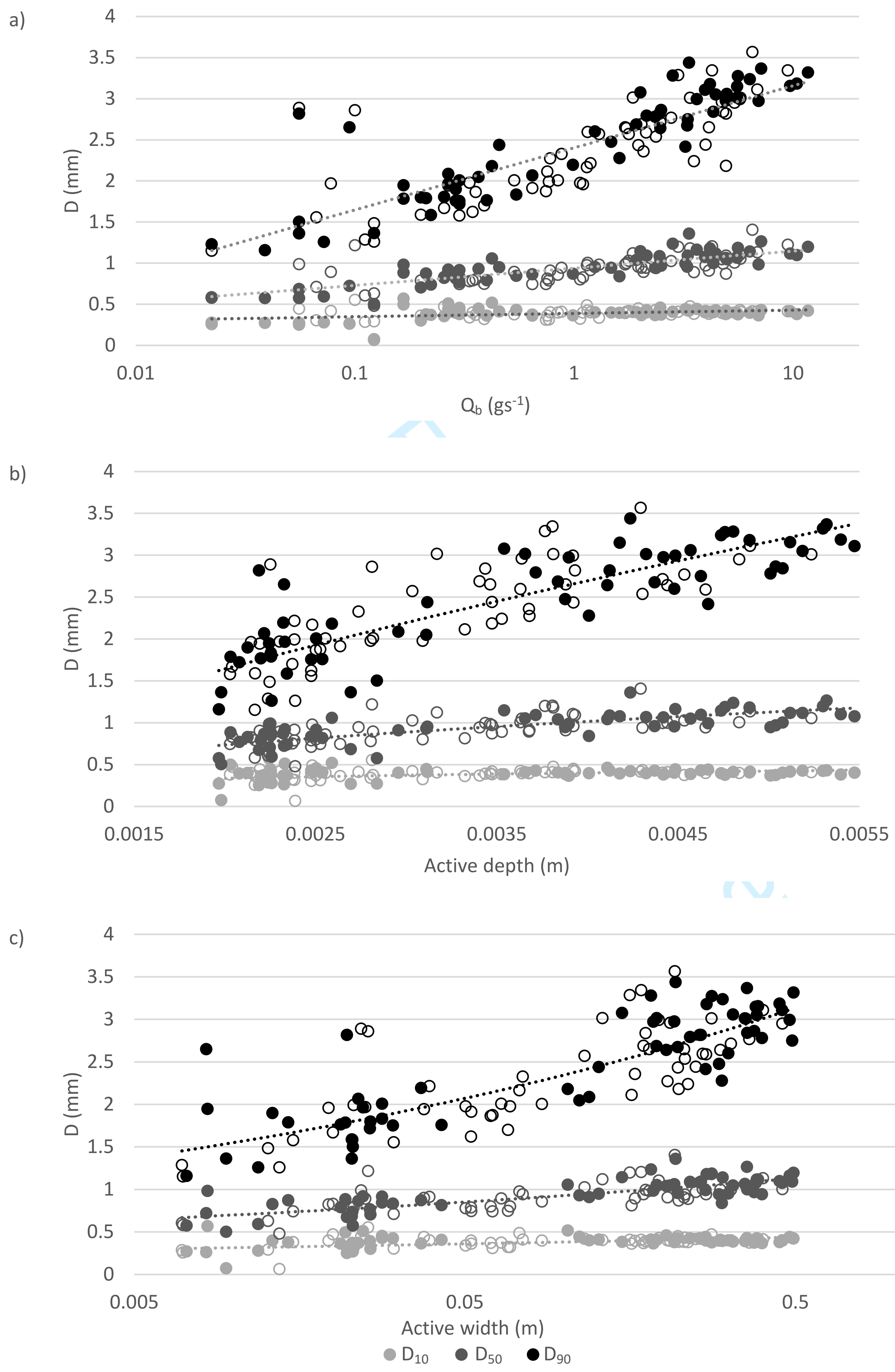
a)
D (mm)
Qb (gs-1)
b)
D (mm)
Active depth (m)
c)
D (mm)
Active width (m)
D10
D50
D90

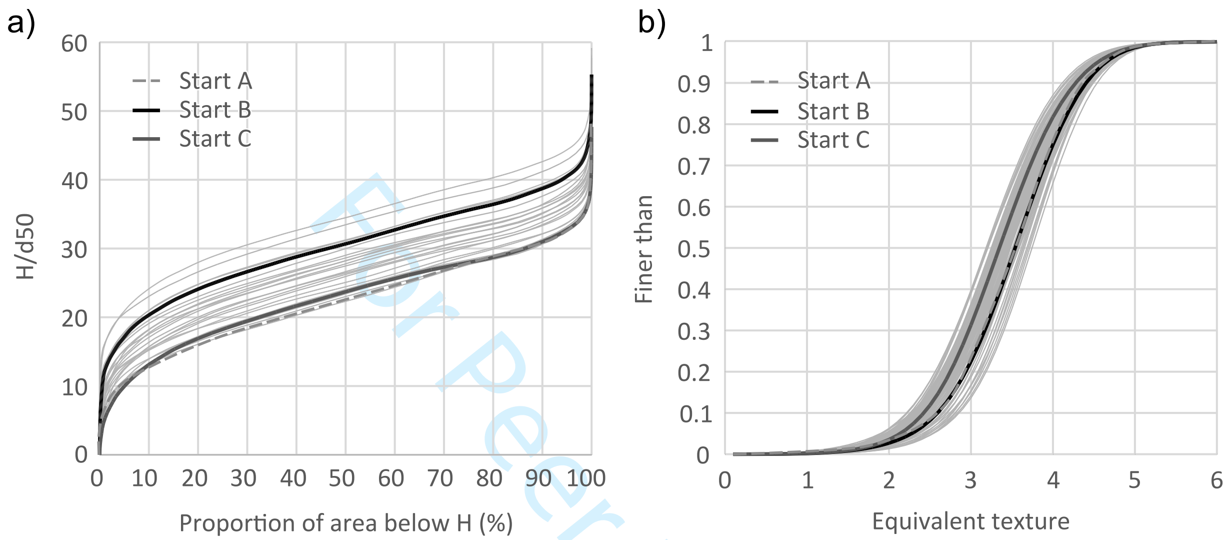
a)
60
50
40
30
20
10
0
H/d50
Start A
Start B
Start C
0 10 20 30 40 50 60 70 80 90 100
Proportion of area below H (%)
b)
1
0.9
0.8
0.7
0.6
0.5
0.4
0.3
0.2
0.1
0
Finer than
Start A
Start B
Start C
0 1 2 3 4 5 6
Equivalent texture

Graphical Information

Title: Evolution of Grain Size Distributions and Bed Mobility during Hydrographs in Gravel-Bed Braided Rivers

Authors: S. Peirce*, P. Ashmore, and P. Leduc

Key findings: Investigation in a physical model of gravel-bed braided river indicated that bed mobility transitioned from partial mobility to selective mobility at discharges ~50% of peak discharge, and approached equal mobility at the highest (i.e., diurnal peak/channel-forming) discharges. The threshold between partial mobility and selective mobility coincided with a threshold for detectable morphological change and substantial increases in bedload transport rates.